DEUTSCHES ELEKTRONEN – SYNCHROTRON

INSTITUT FÜR HOCHENERGIEPHYSIK

DESY 92-176
December 1992

受入
93-2-177
高工研図書室

Test of a Position-Sensitive Photomultiplier for Fast Scintillating Fiber Detector Read-Out

J. Bähr, B. Hoffmann, H. Lüdecke
R. Nahnhauer, M. Pohl, H.-E. Roloff

Deutsches Elektronen-Synchrotron DESY
Institut für Hochenergiephysik IfH, Zeuthen

ISSN 0418-9833

PLATANENALLEE 6 · O-1615 ZEUTHEN

DESY behält sich alle Rechte für den Fall der Schutzrechtserteilung und für die wirtschaftliche Verwertung der in diesem Bericht enthaltenen Informationen vor.

DESY reserves all rights for commercial use of information included in this report, especially in case of filing application for or grant of patents.

To be sure that your preprints are promptly included in the
HIGH ENERGY PHYSICS INDEX,
send them to (if possible by air mail):

DESY
Bibliothek
Notkestraße 85
W-2000 Hamburg 52
Germany

DESY-IfH
Bibliothek
Platanenallee 6
O-1615 Zeuthen
Germany

DESY 92-176
December 1992

ISSN 0418-9833

Test of a position-sensitive photomultiplier for fast scintillating fiber detector read-out

J. Bähr, B. Hoffmann, H. Lüdecke
R. Nahnhauer, M. Pohl, H.-E. Roloff

Deutsches Elektronen-Synchrotron DESY
Institut für Hochenergiephysik IfH, Zeuthen, Germany

October 19, 1992

Abstract

A position–sensitive photomultiplier with 256 anode pixels has been used to read–out scintillating fibers excited by light emitting diodes, electrons from a β-source and a 5 GeV electron beam. Measurements have been done within a magnetic field up to 0.6 T. Tracking and electromagnetic shower detection capabilities of a simple fiber detector have been studied.

1 Introduction

Scintillating fiber detectors are of great interest for future particle physics experiments because of their short response time, good spatial resolution and flexible detector geometry [1]–[3]. A still unsolved problem is however the fast opto–electronical conversion of the scintillator light pulses for a large number of detector channels within reasonable costs. Today one concept is to use image intensifiers in connection with CCD's [4]–[6]. Several thousand detector channels can be handled within one opto–electronic chain in this way. For low rate fixed target experiments first large scale detectors are in preparation [7]. The read–out time is however in the order of some milliseconds and too large for future hadron–collider applications.

Several techniques are under development to realize short read–out times of some ten nanoseconds for scintillating fiber detectors [8]–[11]. Most of these studies aim for LHC and SSC applications and large scale development programmes have been set up. Our own studies are initiated by discussions about a possible application of fiber detectors at the HERA electron–proton collider within the next few years. Therefore we decided to investigate in detail the properties of position–sensitive photomultipliers already available since several years and used or proposed for special fiber detector arrangements [12]–[14].

In the following we describe the test of the position–sensitive photomultiplier (PSPM) Hamamatsu H4140-01 [1] with 256 anode pixels. The device was used in connection with a four layer fiber detector of 1mm diameter fibers allowing track reconstruction for minimum ionizing particles. In chapter 2 we describe the properties of the PSPM, the fiber detector and the geometrical arrangement of our testbeam set–up. Results about measured spatial resolution and efficiencies of the PSPM are given in section 3. Here also the influence of a magnetic field to the PSPM response is discussed. The fiber detector efficiency is studied in detail in section 4 whereas track reconstruction data are presented in section 5. Particle shower detection possibilities of the fiber detector are discussed in section 6. In chapter 7 our conclusions are summarized.

2 Experimental set–up

2.1 The position–sensitive photomultiplier (PSPM)

Several types of position–sensitive photomultipliers are offered by different producers. For a few of them first results of fiber read–out applications have been published [15]–[17]. We decided to use a device with maximum number of pixels able to work in a high magnetic field. Therefore our choice was to test the Hamamatsu PSPM H4140–01.

The PSPM has an uniform photocathode with a quantum efficiency of about 20% at 400nm. The anode is devided in 256 pixels arranged in 16 columns and 16 rows with a pitch of 2.54mm and a sensitive area of 2.34 x 2.34mm^2 (see figure 1). These columns and rows define the x–y–coordinate system which we will use in the further analysis. With 16 dynode stages a gain of 1.5 x 10^6 is reached for a voltage of 2700V decreasing with increasing magnetic field. The cross–talk between different anode pixels is rather large. It decreases in a magnetic field and leads to a three times better spatial resolution in this case as can be seen in figure 2.

To couple 256 fibers of 1mm diameter to the PSPM entrance window we built a suitable mask

[1] HAMAMATSU PHOTONICS K.K., Electron Tube Center, 314-5 Shimokanzo, Toyooka village, Iwata–gun, Shizuoka-ken, 43801,Japan

where the fibers could be glued to. The mask has 256 holes with the same pitch as the anode pixels. It could be moved at the PSPM surface within a frame in x and y direction with a precision better than 10μm. With lower precision also a rotation was possible.

The pulse rise time of the anode signals of the PSPM is 2.7nsec. Therefore restrictions of the time behaviour of a future fiber detector of this type are mainly due to the read–out electronics. This problem has to be solved for every collider detector component and will not be treated in our studies. For our tests we got borrowed the complete read–out boards developed for the L3–fiber detector [12]. The serial output of these boards was digitised by a SIROCCO–II flash ADC using a VME–OS9 online data taking system with a CAMAC interface. Sometimes the amplified sum signal of the last PSPM dynode stage was included in the trigger scheme to increase the PSPM efficiency.

2.2 The fiber detector

The fiber detector was delivered by industry [2]. We had ordered two planes of double layers consisting of 1mm fibers staggered by half a diameter. The length of the scintillating fibers varied between 22 and 32cm. Plastic light guides of 2m length and 1mm diameter were spliced to them [18] to transport the scintillation light to the PSPM. Each double layer consists of 2x200 fibers coherently arranged.

Unfortunately our geometrical demands could not be fulfilled by the producer. Figure 3 shows the endface of the illuminated fibers of the detector part used. Large irregularities are visible. We find an average deviation from the expected fiber position of about 500μm with large fluctuations in different detector parts . Because the main purpose of our investigations was the study of the PSPM properties the results presented in the following are only marginally influenced by this situation. Nevertheless we measured the coordinate of each fiber and used in the following these coordinates to determine the position of particles crossing the detector layers. The precision of our coordinate measurement is about 100μm (see figure 4).

The light guides of 64 fibers of each layer were glued to the PSPM mask. For this purpose the mask was devided in four quadrants, one for each layer. Inside one quadrant the arrangement of fibers to the mask was done randomly to avoid optical cross talk. The two detector planes got separate frames which allowed to use them in arbitrary distance and angle to each other.

At the mask positions (4,4), (4,13), (13,4), (13,13), i. e. at the center of each quadrant, green light emitting diodes have been glued to the light guides for calibration purposes.

2.3 The testrun set–up

At the beginning of our investigations we coupled single scintillating fibers to different positions of the PSPM mask. These fibers were excited by a Sr^{90} – β–source. The trigger signal was formed in this case by a coincidence of the signals from a small scintillator below the fiber and the sum signal of the PSPM.

A more complex set–up was used during a testrun in a 5 GeV electron beam at DESY in Hamburg (see figure 5). To test the PSPM response in dependence of a magnetic field the multiplier was placed inside a solenoid allowing fields up to about 1Tesla. To work properly the

[2] OPTECTRON S.A., B.P. 535, F–91946 Les Ulis,France

PSPM axis should be parallel to the direction of the field. Therefore the PSPM support could be fully rotated to allow correct alignment.

In front of the magnet a support for the two fiber detector planes and the trigger system was installed which allowed again two independent rotations for adjustment to the beam line. The two detector planes are installed transverse to the beam with a minimum distance of 2cm. They could be moved independently of each other in vertical and horizontal direction. The connection to the PSPM was done by the 2m long flexible light guides.

The trigger for beam particles was formed by demanding a coincidence of four scintillation counter signals covering a transverse space region of $1 \times 1\text{cm}^2$ at the detector surface. In a second part of the run a special halo–counter with a 5mm hole was used in addition.

To test the preshower properties of the fiber detector a 1cm thick lead–plate could be installed between the fiber detector planes.

3 PSPM spatial resolution and efficiency

3.1 Single fiber response

In a first step of our investigation we coupled one 1mm scintillating fiber to a certain position of the otherwise empty PSPM mask to avoid problems with optical cross talk or double hits caused by other phenomena. The mask was roughly adjusted to the corresponding PSPM anode pixels. The fiber was exited by electrons from a β–source as described in section 2.3. The PSPM high voltage was set to 2500V. It had to be increased later on to the maximum value of 2700V to increase the efficiency for the detection of minimum ionizing particles.

In the following we give only a qualitative discussion of the PSPM response to a single fiber light signal to demonstrate the main problems for a detector application. A quantitative calculation of the most important parameters will be given in sections 3.3 and 3.4. The anode pixel amplitude is measured as the content of the corresponding flash ADC–channel where a previously measured pedestal for this channel is subtracted. The pedestal appears to be very stable for long periods with a full width at half maximum of about 10 ADC-counts.

In figure 6 we show the distribution of amplitude maxima for 4540 single fiber events. The amplitudes fit well in the ADC range up to 1024 counts. Two peaks are visible. Events without fiber signals concentrate in the region below 50 counts and can be clearly separated from real signals which give a peak at about 170 ADC counts.

After a general amplitude cut of 50 counts 3886 events remain. For these events we show the average amplitude distribution per amplitude pixel in figure 7a. As can be seen this is a rather broad distribution. The pixel (8,14) where the fiber is adjusted to gives clearly the maximum response which is however only about 10 percent of the total signal. These effect is due to two different sources. At first the cross talk between the anode pixels in one events is large, at second the maximum position of the amplitude varies from event to event. This is demonstrated in figure 7b where one can see that only for 60% of all events the maximum is at the right position (8,14). The nearly 20% contribution of the neighbouring fiber (9,14) could be possibly diminished by more careful adjustment of the fiber mask. Nevertheless even a small percentage of far away hits is observed.

It is assumed up to now that the relative anode sensitivity is the same for every anode pixel. As will be shown in the next section this is not true. To measure the anode pixel sensitivity is

however very complicated because of the large cross talk between all anodes.

3.2 Calibration

As a consequence of the large cross-talk, the measured amplitude of one anode pixel is due to contributions from light in a large neighbouring region at the PSPM surface if the whole PSPM is illuminated. Therefore pixels at the boundary can not have the same amplitude as those in the center of the PSPM because their neighbouring region is restricted. To take into account this effect, Hamamatsu provided a table which corrects also for local non-uniformities. The table content is distributed in figure 8a. It was measured at 2000V using a Wolfram-lamp to illuminate the PSPM. Since the gain of the PSPM increases considerably with increasing high voltage, we measured a correction table at a high voltage of 2700V where most of our data are taken (see fig. 8b). To do that we illuminated the photocathode of the PSPM with a pulsed green LED at a distance of 60cm. Our result is not directly comparable with that given by Hamamatsu because our measurement corrects also for variations in the efficiency of the read–out electronics of different pixels. This explains the larger fluctuations of the data shown in figure 8b compared to figure 8a.

The influence of the different correction tables was studied using cosmic particles. The two detector planes with each two fiber layers are placed between two trigger counters which covered an area of about $6 \times 6\text{cm}^2$. We analyzed about 2000 events. The measured amplitudes were uniformity corrected. For each event we used the maximum amplitude per detector layer as the position, where the cosmics particle hits the layer (a threshold cut of 30 counts was applied for the corrected amplitudes). Applying the different correction tables the resulting distributions of maxima are shown in figures 8c and 8d. The events should be equally distributed over all PSPM anode pixels. This is only approximately true for our limited statistics. Nevertheless both distributions look similar to each other.

3.3 Hit determination

The use of a PSPM for the read–out of a fiber track detector demands to identify a fiber which was hit by a particle with high efficiency. To measure this efficiency in our configuration we use the four LED–fibers mentioned in section 2.2. We adjusted the mask containing 256 fibers to the photocathode of the PSPM demanding for LED–fiber (4,4) a maximum amplitude at the right position and a symmetrical cross talk. For the remaining LED–fibers these parameters were also optimized. However even with a mask accuracy of about 100μm with respect to the anode pixel array it was impossible to adjuste all four LED–fibers with the same precision. This can be explained by geometrical distortions caused by the opto–electronic scheme used.

To reconstruct the LED–fiber coordinates we used the position of the maximum amplitude in the given quadrant of the PSPM. A typical event and the fit result of a two–dimensional gaussian distribution for this event are shown in figures 9a and 9b, respectively. It is easy to see that the maximum amplitude of the event is at the wrong position (3,4), which means that we loose this event. For the sum of thousand events the predicted position (4,4) is reproduced very well, as can be seen from figure 9c and 9d. The two–dimensional gaussian fit to the distribution in figure 9d yields a standard deviation of 1.1 PSPM–units. This corresponds to a total width of 5.6 mm which roughly agrees with the design value of 6.0mm given by Hamamatsu.

The PSPM–efficiency is defined as the number of correctly identified hits to the total number of hits in this quadrant. For the four LED–fibers it is summarized in table 1 for a high voltage of 2700V. There we present also the percentage of events which are misidentified by one or more

anode pixels. As can be seen the largest effiency is measured for the most carefully adjusted LED–fiber (4,4). The average pixel efficiency comes out to be about 46%, however one should keep in mind that it varies over the PSPM–plane from 30% to 70%.

Table 1 shows also that there are long range effects of the order of 10%. The column denoted by "rest" gives the number of hits displaced into another quadrant of the PSPM. About 2% of the hits in one detector layer appear as hits in one of the three other layers.

As already mentioned in section 3.2, the PSPM–response changes with varying high voltage. Figure 10 shows the reconstruction efficiency of hits in dependence of the PSPM voltage for all four LED–fibers. With increasing high voltage this efficiency increases considerably. Therefore we used the maximum allowed value of 2700 V for data taking.

3.4 Influence of a magnetic field

To use the PSPM in a magnetic field we first aligned the multiplier axis parallel to the field direction. Afterwards we made measurements in this position and with an angle of about 30 degrees between these directions and found no big differences for the results of both data. The field strength was measured directly at the PSPM position.

In figure 11a we show the amplitude distribution for the sum of thousand events for LED–fiber(4,4) observed in a magnetic field of 0.1 T. As could be expected from the producers data (figure 2) the spread of the distribution is smaller than without a magnetic field shown in figure 9d. The average half width of the single event amplitude distributions of LED–fibers is given in figure 11b for different magnetic fields. Starting with a total amplitude width of 5.6mm without a magnetic field a value of about 1.8 mm is reached for a field of 0.6T. Our measurements confirm the data given in figure 2.

Unfortunately one can not profit from the lower cross talk and improved spatial resolution. In figure 11c we show the measured hit efficiency in dependence of the magnetic field strength for the four LED–fibers. More detailed data are presented in table 2 for a field of 0.1T. As can be seen the number of correctly determined hit positions decreases dramatically for fields of a few hundred Gauss and increases above 0.1 T to a plateau value. Obviously this is due to global distortions introduced by the magnetic field which are probably compensated at higher field values by a focussing effect of the field. This seems to be confirmed by the results given in figure 12a-d where the average hit position of all four LED fibers is shown for different magnetic fields. At low values of the field the difference to the position without field is largest coming back in smaller and smaller steps with increasing field value.

4 Fiber detector efficiency

The detection efficiency of a fiber detector for minimum ionizing particles was measured using the testrun set-up described in section 2.3 in a 5GeV e^--beam at DESY. The data were taken without a magnetic field.

The PSPM delivers in addition to the pixel–response the sum signal of the last dynode. It allows to cut empty events without any fiber signal. Table 3 summarizes the calculated efficiencies for two data samples. In sample 1 we excluded the sum signal from the trigger scheme, whereas for sample 2 it was used. The comparison of the two columns shows the increase of efficiency. For each detector layer we oserve the sharp beam profile. In table 3 we counted for each event in all four PSPM–quadrants (layers) hits above an amplitude threshold of 30 ADC counts. The

corresponding numbers are given normalized to the total number of about 15000 events in both data samples described. The efficiency for sample 1 comes out to be in average $\epsilon^{FIB} = 0.64$ for each of the four detectors. The expected efficiency to see a hit in all of the four fiber layers is consequently $\epsilon^{FIB}_{tot} = 0.18$ in agreement with the measured value given in the last row of table 3. For the enriched data sample 2 the single fiber efficiency is larger by a factor of 1.2 in comparison to the unbiased data. This results in about twice as much events with hits in all four fiber layers.

Due to inhomogenities in the fibers, differences in the optical coupling etc. the fiber efficiency is expected to vary for different regions of the detector. This is shown in figure 13a for data taken under the same condition as for sample 2 above. It shows that the fiber efficiency varies in the order of 10% across the detector. The quality of the four layers differs considerably.

Due to light attenuation in the fibers their response changes in dependence of the excitation point. The corresponding results are given in figure 13b for all four fiber layers. They agree with an attenuation lenght of about 25cm measured for single fibers of the same type.

5 Track reconstruction

To measure an unbiased track resolution for a straight line fit to the data we need four hits per particle crossing our detector arrangement. The number of four hit events was found to be 4% of the total data sample. This efficiency can also be calculated as the product of the fiber efficiency ϵ^{FIB} and the efficiency to get the right PSPM–hit. The values given in tables 1 and 3 lead to a calculated 4–hit efficiency of about 2% in rough agreement with the measured value.

The track resolution for a straight line fit to four hit events is shown in figure 14a. The average track point precision comes out to be about 600 μm. The result is explained by the large irregularities of the fiber arrangement in the corresponding layers (see section 2.2). That we measure beam tracks is proven by the narrow distribution for the track slope parameter shown in figure 14b.

6 Pre–shower detection

The use of scintillating fibers for pre-shower detection was already successfully tested [4]. To study the shower detection possibility of our set–up we inserted a 1cm thick lead plate (1.8 radiation lengths) between the two fiber detector planes. In this configuration the first two fiber layers are used for track identification and layers 3 and 4 for shower detection.

The detector was exposed to a 5GeV electron beam using the same trigger conditions as those described for data sample 2 in section 4. The corresponding results are summarized in table 4. The fiber detector efficiency for layers 1 and 2 is about the same as measured in the previous runs (compare table 3). In contrast the efficiency for layers 3 and 4 is much larger than measured without the lead plate and comes already close to 100 %. This is probably due to low energetic electrons produced in the electromagnetic cascade within the lead. This conclusion is confirmed by the other results shown in table 4 which are derived from events where all four detector layers give signals.

The average number of hits $< N_h >$ increases considerably for the layers behind the shower material. That this value is larger than one for the first two layers is due to an overlap of the PSPM response between layers 2 and 3 and layers 1 and 4 due to the large cross talk between neighbouring anode pixels. This influences all following results but could be avoided for a real

detector application where only one fiber layer should be coupled to one PSPM. The average maximum amplitude per detector $<A_m>$ is about a factor three larger for the shower detection layers due to the higher ionization loss of low energetic particles. The total amplitude sum per detector layer ΣA_i is influenced both by the larger number of hits and the higher energy deposit. The corresponding result is given in table 4 and shown in more detail in figure 15. The slightly larger signals in layer 4 compared to layer 3 may be a reflection of the transverse shower development.

The pre–shower detection capability for our simple detector configuration is already rather large. This is illustrated in figure 16 where the event distribution of the ratio of amplitude sums for the layers in front of the lead plate and behind it is shown. As can be seen only for about 2.5% of all events one would fail to identify the electromagnetic cascade. More efficient fibers and more layers on both sides of the shower material would diminish this number further. Unfortunately we were not able to investigate the detector response for incoming photons and pions of similar energies as the electrons used in this study because no particle beams of this type where available to us.

7 Summary and conclusions

We tested a 256 multianode pixel photomultiplier for its applicability as read-out device for a scintillating fiber tracking detector. Our measurements confirm published data about cross-talk and spatial resolution of this device. We found however that the efficiency to detect a fiber emitting light at a certain position of the photocathode at the right PSPM anode pixel is smaller than 50 percent. This is still much too low for a real fiber detector application.

The use of the same photomultiplier within a magnetic field decreases the cross talk and improves the spatial resolution. It leads however to image distorsions which decrease the fiber detection efficiency further.

An electromagnetic shower produced by 5GeV electrons in 1cm of lead is detected in a single fiber layer with nearly 100% efficiency.

In the near future an improved version of the photomultiplier investigated here is available and will be tested.

Acknowledgements

We gratefully acknowledge the kind support of A.Pevsner and J.Spangler from Johns Hopkins University by borrowing us several complete readout boards developed originally for the L3-fiber detector at CERN. In an early stage of the programme we got help from S. Merzlyakov of the Laboratory of Nuclear Problems of JINR Dubna who was involved in setting up the data taking chain for the position–sensitive photomultiplier. Finally we profitted from discussions with K.Hiller and other colleagues of our institute.

References

[1] Proceedings of the "Large Hadron Collider Workshop", Aachen 1990, Eds. G. Jarlskog und D. Rein, CERN 90-10.

[2] Proceedings of the "Symposium on Detector Research and Development for the Superconducting Super Collider", Fort Worth, 1990, Eds. T. Dombeck, V. Kelly, G. P. Yost.

[3] Proceedings of the "Workshop on Application of Scintillating Fibers in Particle Physics", Blossin 1990, Ed. R. Nahnhauer.

[4] R. Ansorge et al., Nucl. Instr. and Meth. A 265 (1988) 33.

[5] M. Adinolfi et al., Nucl. Instr. and Meth. A 311 (1992) 91.

[6] M. Gruwe et al., "A Set Up for Precise Measurements of Scintillating Fiber Bundles Using an Opto-Electronic Readout Chain and a Silicon Micro-Strip Detector System", DESY 92-088 (1992) to appear in Nucl. Instr. and Meth.

[7] N. Armenise et al., "A new search for $\nu_\mu - \nu_\tau$ oscillations", CERN - SPSC/90-42(1990).

[8] T. Gys et al., "Opto-electronic delay tubes" in Proceedings of the "Large Hadron Collider Workshop", Aachen 1990; Eds. G. Jarlskog and D. Rein Vol. 3, 261.

[9] J. P. Fabre et al., Rev. Phys. Appl. 24 (1989) 1019.

[10] M. Atac et al., Nucl. Instr. and Meth. A 314 (1992) 56.

[11] M. Atac et al., Nucl. Instr. and Meth. A 320 (1992) 155.

[12] H. Akbari et al., Nucl. Instr. and Meth. A 302 (1991) 415.

[13] K. Kuroda et al., Nucl. Instr. and Meth. A 300 (1991) 259.

[14] V. Agoritsas et al., "Topological Trigger Device using Scintillating Fibers and Position-Sensitive Photomultipliers" in Proceedings of the "Large Hadron Collider Workshop", Aachen 1990, Eds. G. Jarlskog and D. Rein, Vol 3, 265.

[15] C. Jeanney et al., "Test on a Position-Sensitive Multichannel Photomultiplier Tube", Saclay - DPhPE 91-07.

[16] M. Salomon "New Measurements of Scintillating Fibers Coupled to Multianode Photomultipliers" in Proceedings of Nucl. Sci. Symp., Santa Fe, 1991, Vol.1, 346

[17] S. Majewski et al., "Studies of Position-Sensitive Photomultipliers for Scintillating and Waveshifting Fiber Readout" in Proceedings of Nucl. Sci. Symp., Santa Fe, 1991, Vol.1, 324

[18] G. Apollinari et al., Nucl. Instr. and Meth. A 311 (1992) 520.

Table Captions

Tab. 1 PSPM anode pixel displacement for four fibers excited by light emitting diodes.

Tab. 2 PSPM anode pixel displacement for the same fibers as in table 1 but for a magnetic field of B = 0.1 T.

Tab. 3 Fiber efficiencies for all detector layers measured for sample 1 without PSPM sum signal in the event trigger scheme. In sample 2 the signal is included in the trigger condition with a threshold cut of 50 mV.

Tab. 4 Fiber efficiency, average number of hits, average maximum amplitude and amplitude sum for all detector layers for a data run where a lead plate is inserted between layers 2 and 3.

Figure Captions

Fig. 1 Top and bottom view of the position-sensitive photomultiplier HAMAMATSU H4140–01 and the corresponding coordinate system used throughout the paper (rows of anode pixels with index I give y-coordinate, columns with index J give x-coordinate).

Fig. 2 Spatial resolution and cross talk for the HAMAMATSU H4140–01 in dependence of the magnetic field strength as given by the producer.

Fig. 3 Transverse view of the four fiber layers of the OPTECTRON fiber detector for the detector part used.

Fig. 4 Precision of the fiber coordinate measurement for the OPTECTRON detector. The fiber diameter is 1mm.

Fig. 5 Photo and scetch of the fiber detector arrangement in the DESY 5 GeV electron beam.

Fig. 6 Maximum amplitude per event for a single fiber placed on the PSPM photocathode exposed to a β-source:

Fig. 7 Same arrangement as in figure 6 : a.) average amplitude distribution for 1000 events, b.) position of maximum amplitude per event for the same data. x-y coordinates given in PSPM-units.

Fig. 8 Results for different anode pixel efficiency tables : a.) HAMAMATSU efficiency table measured at a high voltage of 2000 V, b.) own measured table at a high voltage of 2700 V, c.) and d.) show the corresponing corrected data of a cosmic particle run where a flat distribution is expected. x-y coordinates given in PSPM-units.

Fig. 9 Fiber at photocatode in front of anode pixel (4,4) illuminated by a light emitting diode : a.)amplitude distribution of a single event, b.) same distribution fitted by a two-dimensional gaussian, c.) and d.) same as a.) and b.) for the sum of thousand events. x-y coordinates given in PSPM-units.

Fig. 10 Hit reconstruction efficiency for four fibers illuminated by light emitting diodes in dependence of PSPM high voltage.

Fig. 11 Magnetic field dependence of some PSPM parameters : a.) amplitude distribution for sum of events for a magnetic field of B = 0.1 T fitted by a two-dimensional gaussian, x-y coordinates given in PSPM-units, b.) half width of event amplitude distributions in dependence of the magnetic field strength, c.) hit detection efficiency for the same LED- fibers as in figure 10 in dependence of the magnetic field strength.

Fig. 12 Average measured LED-fiber position for four LED-fibers in dependence of the magnetic field strength.

Fig. 13 Dependence of fiber efficiency on a.) different beam positions across the detector layers, b.) different beam positions along the fibers.

Fig. 14 Track reconstruction parameters for four-hit tracks : a.) measured resolution, b.) fitted track slope.

Fig. 15 Amplitude sum per detector layer : a.) and b.) for layers in front of a 1 cm thick lead plate, c.) and d.) for layers behind this plate.

Fig. 16 Ratio of amplitude sums of layers in front and behind 1 cm of lead.

B = 0.0T					
LED-fiber position	# Anode pixels displaced [%]				
	0	1	2	3,4=long range	rest
(4,4)	63.9	24.4	5.0	4.6	2.1
(13,4)	35.4	47.6	6.1	6.3	4.6
(4,13)	44.5	41.5	6.0	6.8	1.2
(13,13)	41.2	38.5	7.1	11.1	2.1
average	46.2	38.0	6.1	7.2	2.5

Table 1

B = 0.1T					
LED–fiber position	# Anode pixels displaced [%]				
	0	1	2	3,4=long range	rest
(4,4)	57.5	31.6	4.2	6.2	0.2
(13,4)	13.6	71.1	5.4	8.2	1.7
(4,13)	23.3	61.1	5.4	9.7	0.5
(13,13)	13.3	55.0	14.3	15.9	1.5
average	26.9	54.7	7.3	10.0	1.1

Table 2

	Fiber detector efficiency ε^{FIB} [%]	
	Sample 1	Sample 2
ε_1^{FIB}	64	78
ε_2^{FIB}	57	71
ε_3^{FIB}	68	81
ε_4^{FIB}	66	81
ε_{tot}^{FIB}	18	34

Table 3

Det	ε^{FIB}[%]	$< N_h >$	$< A_m >$	ΣA_i
1	78	1.74	185	3653
2	69	1.59	175	4011
3	98	2.44	536	10440
4	99	2.86	617	12350

Table 4

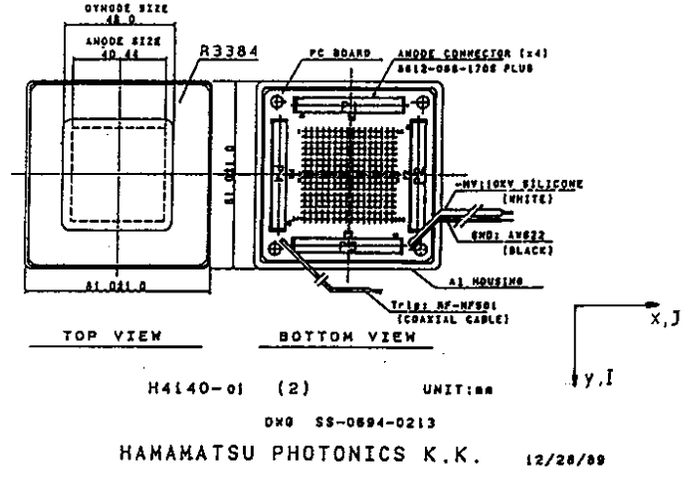

Fig. 1

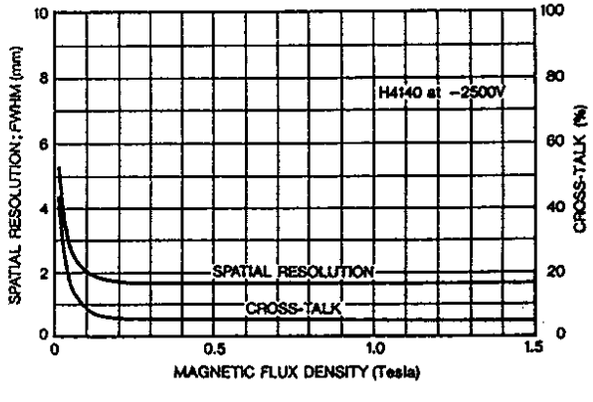

Fig. 2

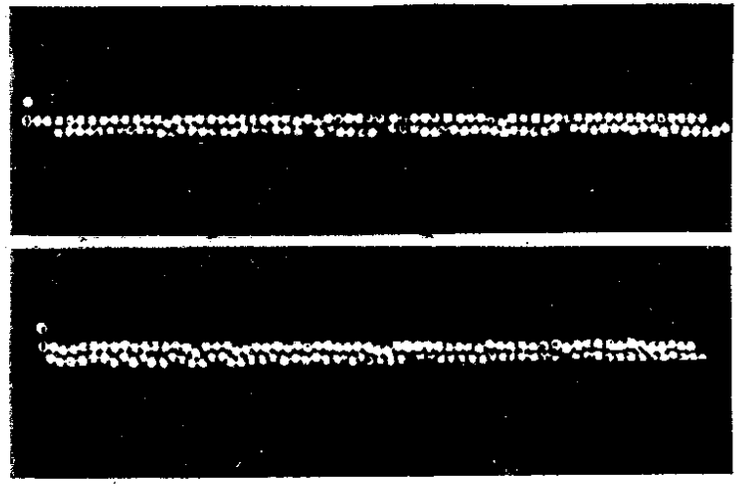

Fig. 3

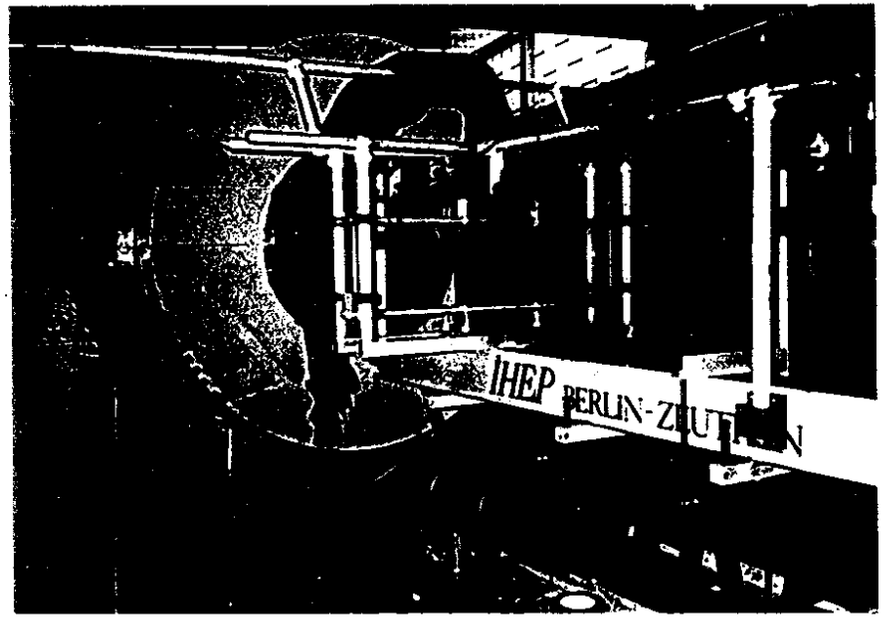

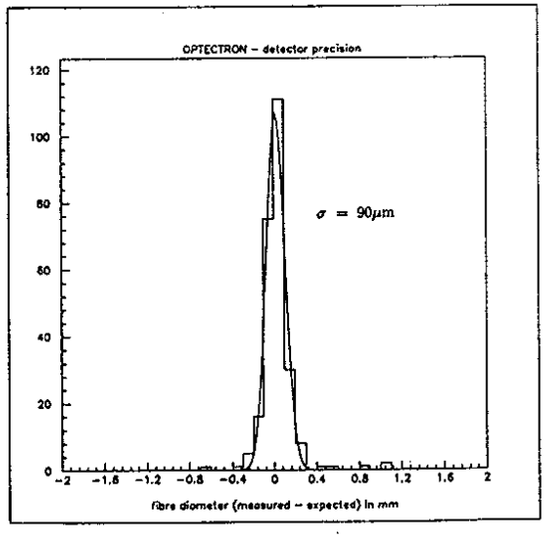

Fig. 4

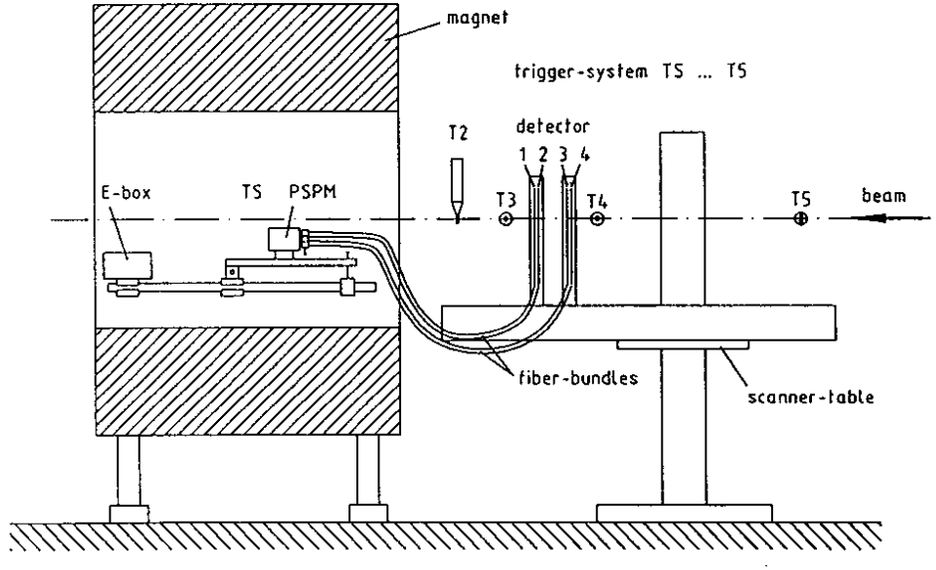

Fig. 5

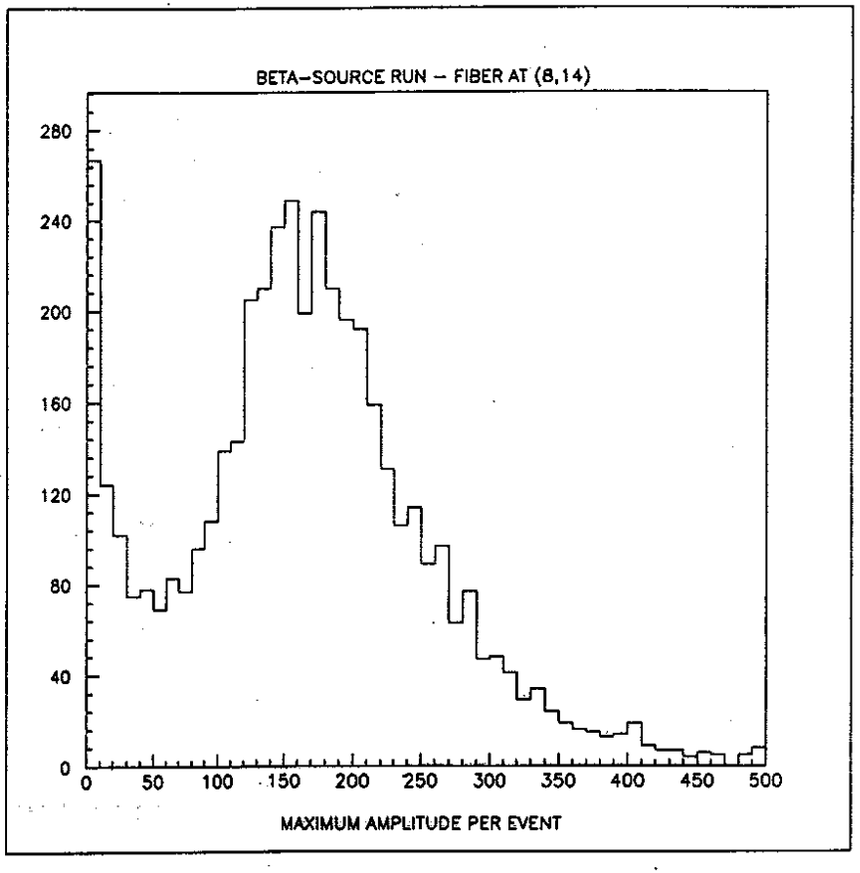
BETA–SOURCE RUN – FIBER AT (8,14)
280
240
200
160
120
80
40
0
0
50
100
150
200
250
300
350
400
450
500
MAXIMUM AMPLITUDE PER EVENT

Fig. 6

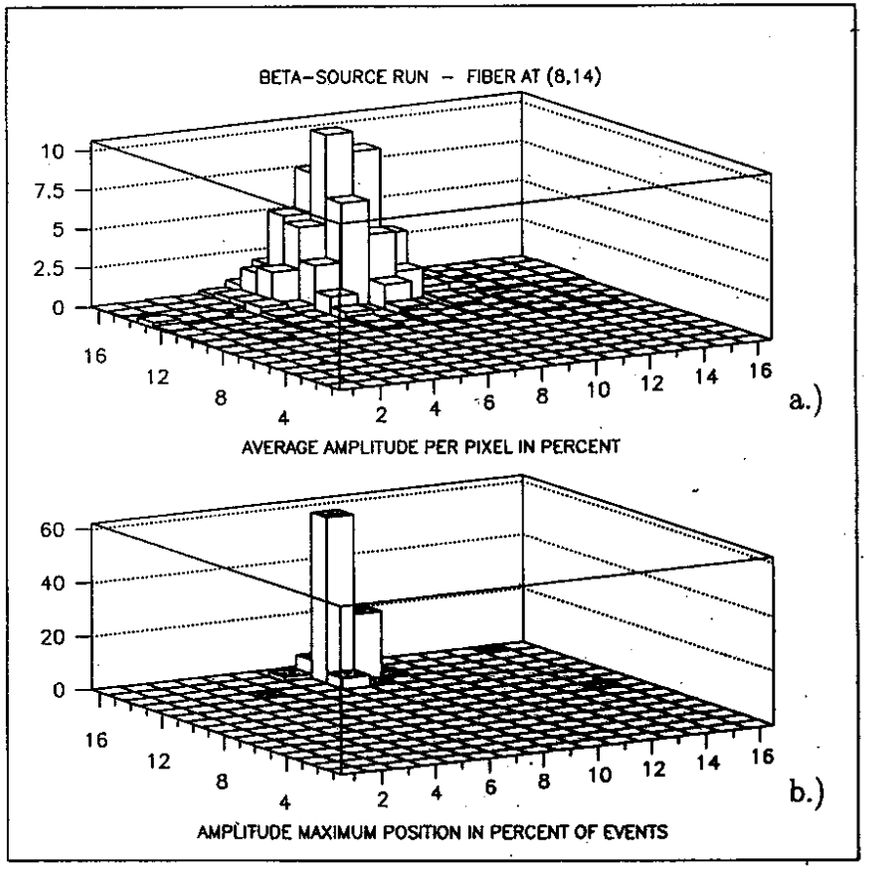
BETA–SOURCE RUN – FIBER AT (8,14)
10
7.5
5
2.5
0
16
12
8
4
2
4
6
8
10
12
14
16
a.)
AVERAGE AMPLITUDE PER PIXEL IN PERCENT
60
40
20
0
16
12
8
4
2
4
6
8
10
12
14
16
b.)
AMPLITUDE MAXIMUM POSITION IN PERCENT OF EVENTS

Fig. 7

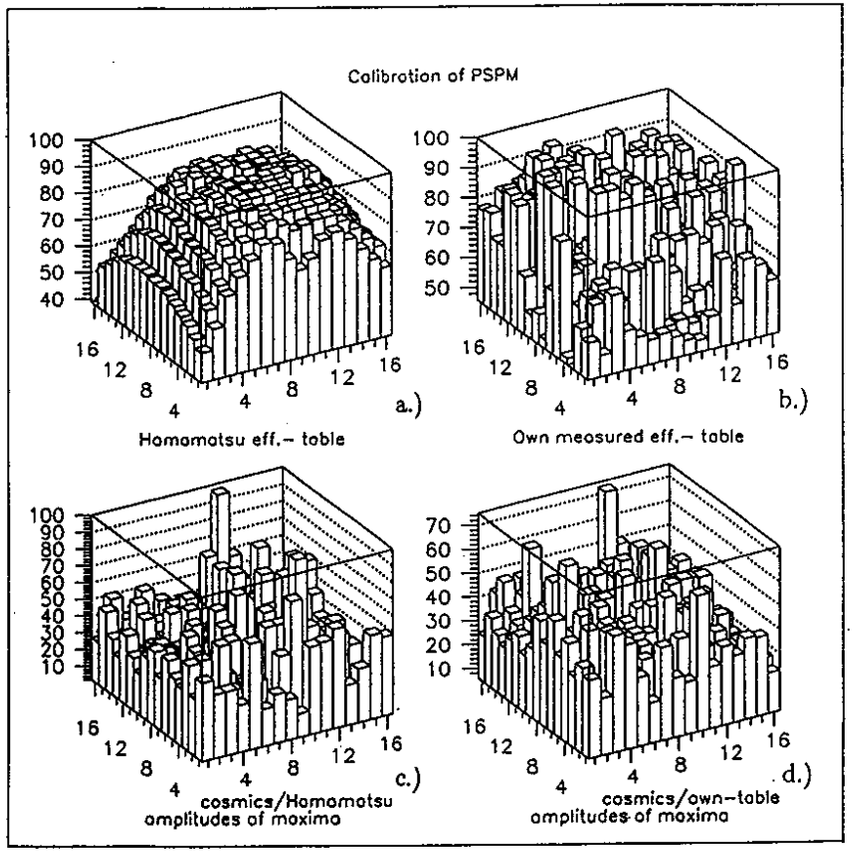
Calibration of PSPM
a.)
Homamatsu eff.– table
b.)
Own measured eff.– table
c.)
cosmics/Homamatsu
amplitudes of maxima
d.)
cosmics/own–table
amplitudes of maxima

Fig. 8

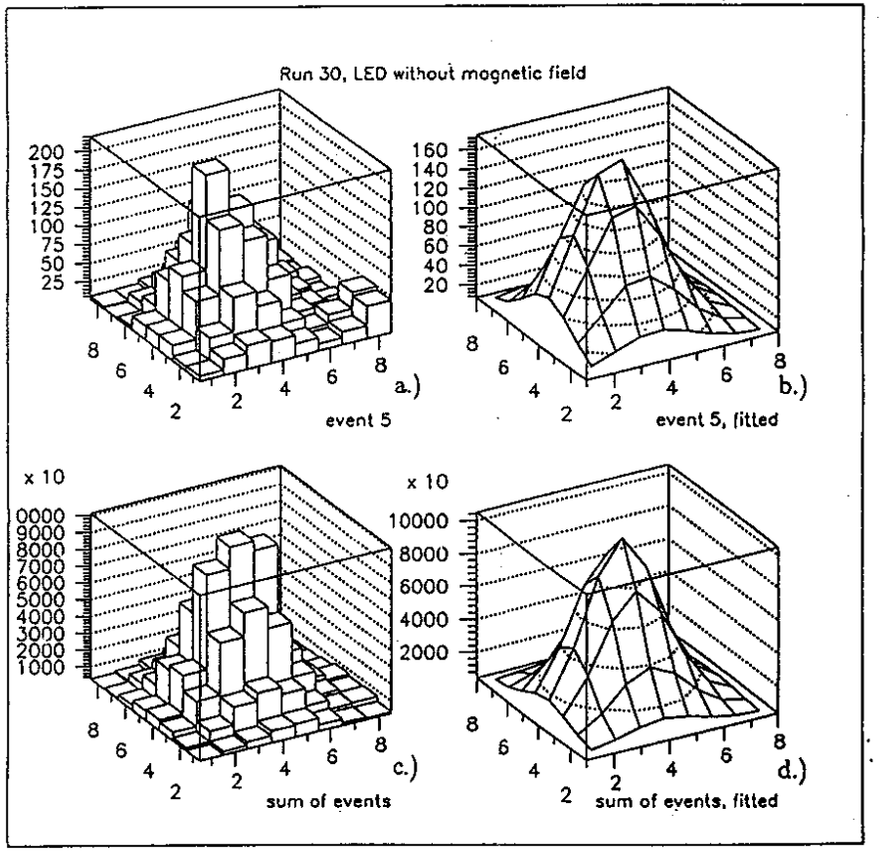
Run 30, LED without magnetic field
a.)
event 5
b.)
event 5, fitted
x 10
c.)
sum of events
x 10
d.)
sum of events, fitted

Fig. 9

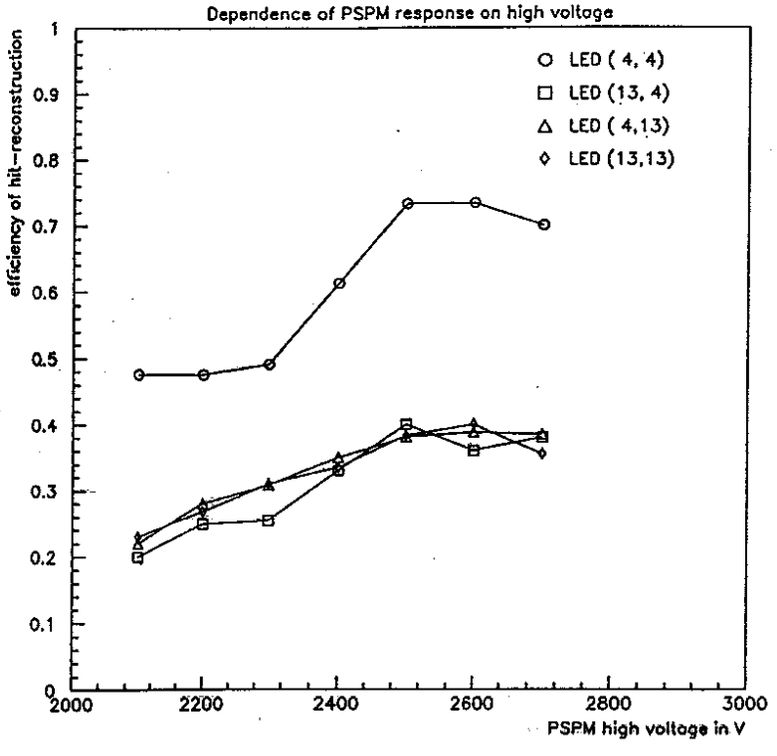
Dependence of PSPM response on high voltage
efficiency of hit-reconstruction
LED (4, 4)
LED (13, 4)
LED (4,13)
LED (13,13)
PSPM high voltage in V

Fig. 10

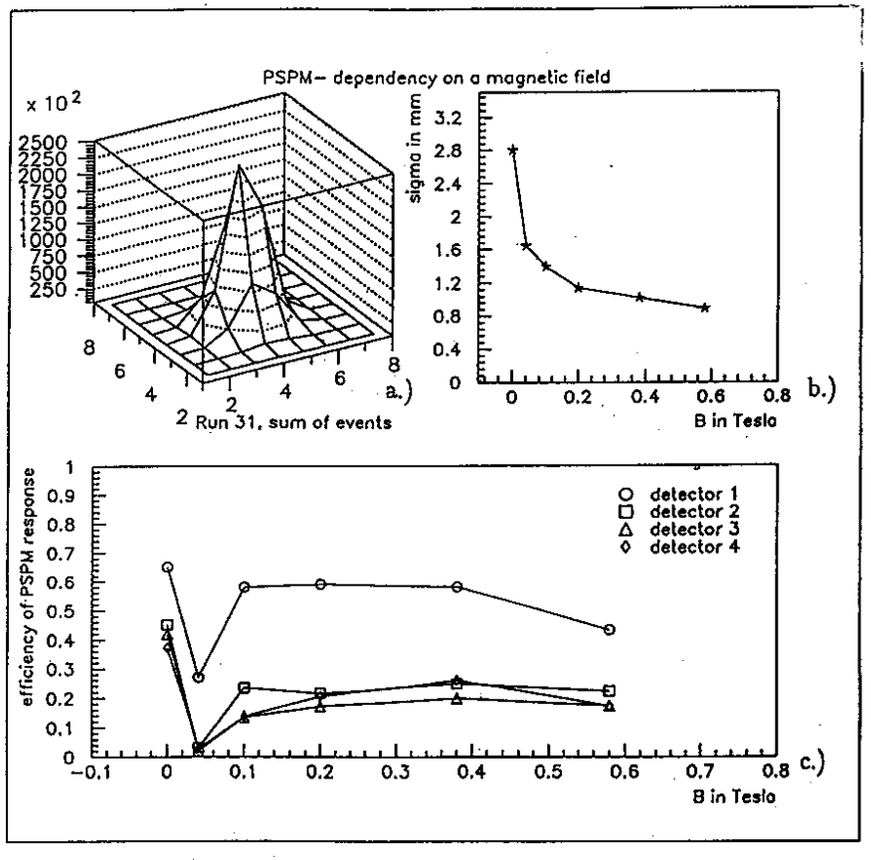
PSPM– dependency on a magnetic field
x 10^2
a.)
Run 31, sum of events
sigma in mm
b.)
B in Tesla
efficiency of PSPM response
detector 1
detector 2
detector 3
detector 4
c.)
B in Tesla

Fig. 11

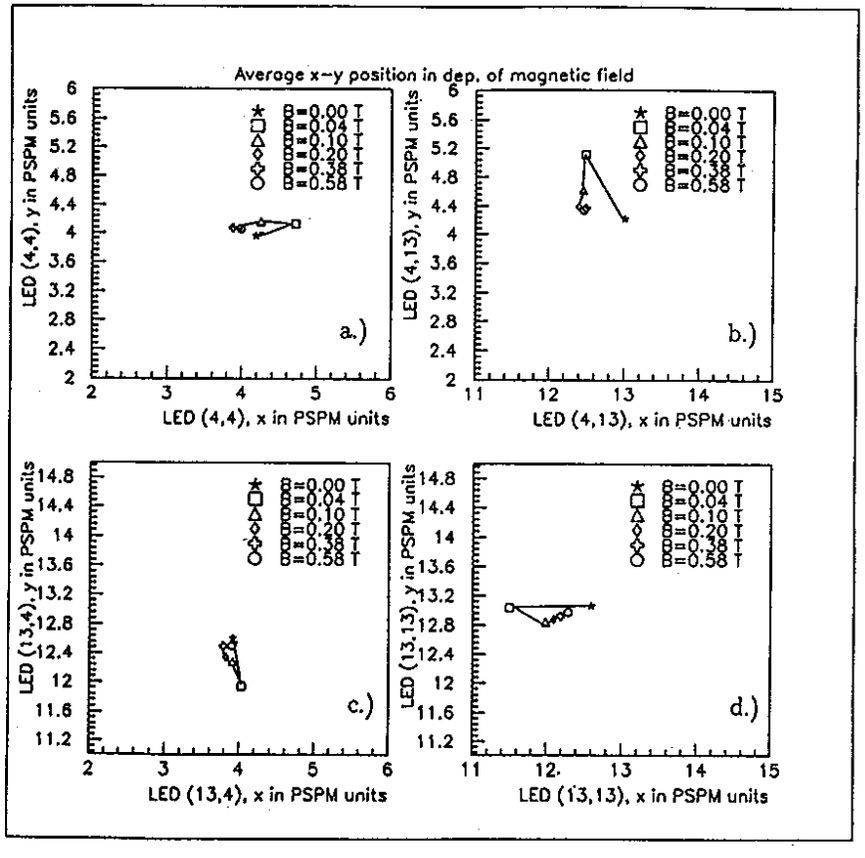
Average x-y position in dep. of magnetic field
B=0.00 T
B=0.04 T
B=0.10 T
B=0.20 T
B=0.38 T
B=0.58 T
a.)
b.)
c.)
d.)
LED (4,4), y in PSPM units
LED (4,4), x in PSPM units
LED (4,13), y in PSPM units
LED (4,13), x in PSPM units
LED (13,4), y in PSPM units
LED (13,4), x in PSPM units
LED (13,13), y in PSPM units
LED (13,13), x in PSPM units

Fig. 12

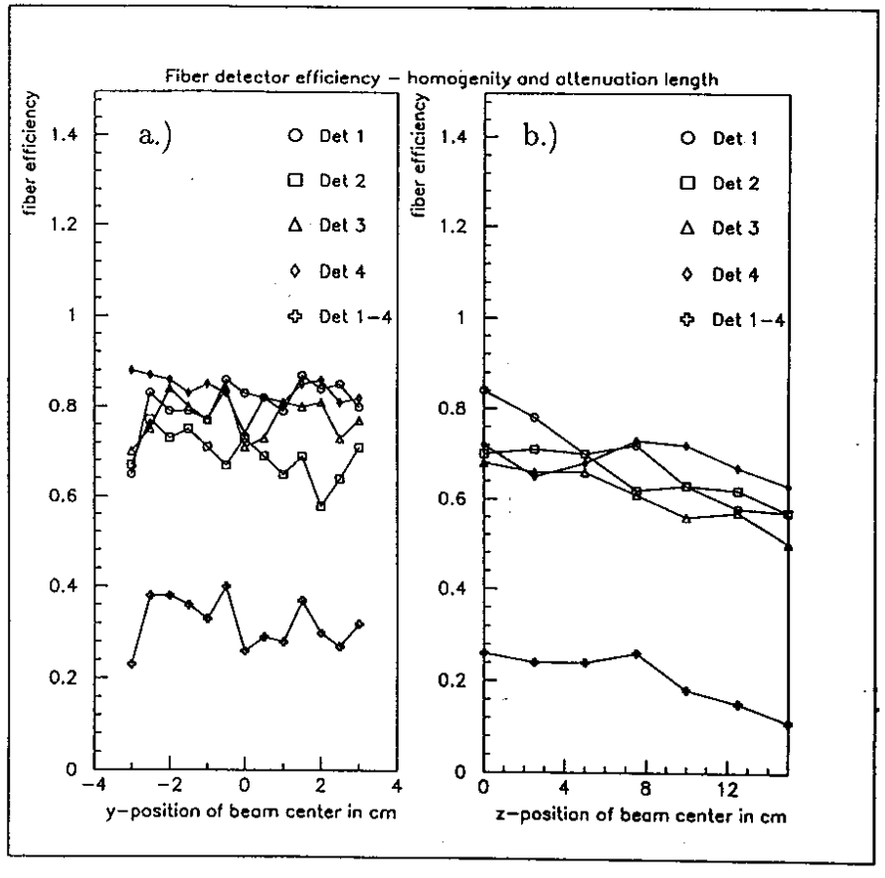
Fiber detector efficiency – homogenity and attenuation length
a.)
b.)
Det 1
Det 2
Det 3
Det 4
Det 1–4
fiber efficiency
y–position of beam center in cm
z–position of beam center in cm

Fig. 13

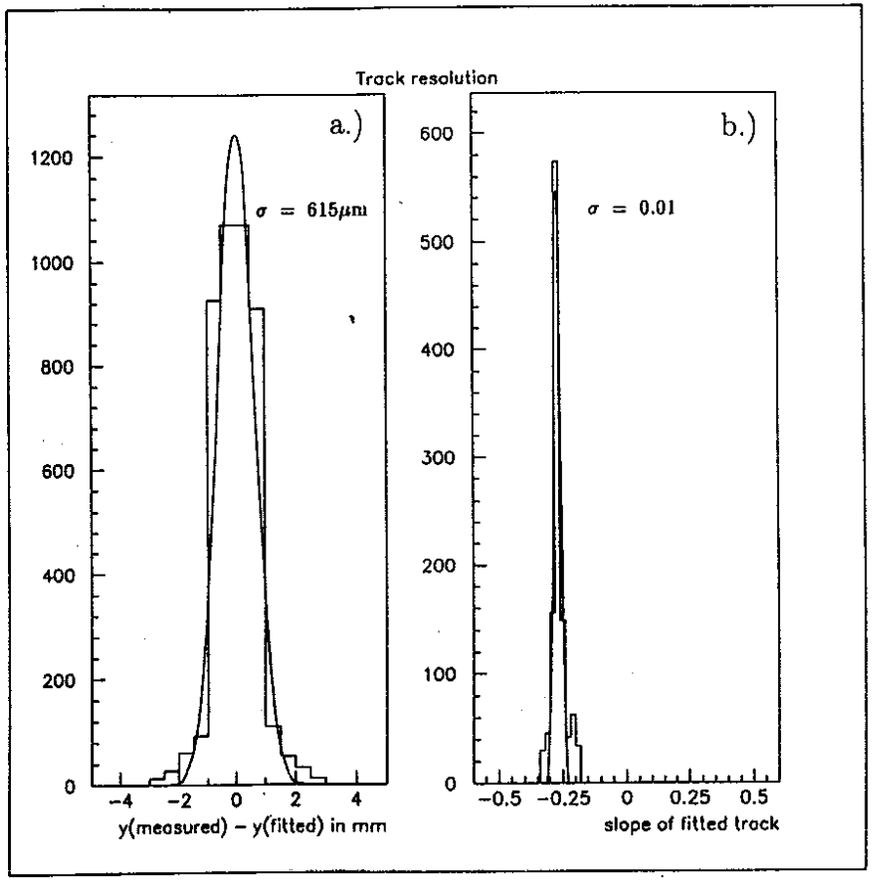
Track resolution
a.)
σ = 615μm
y(measured) – y(fitted) in mm
b.)
σ = 0.01
slope of fitted track

Fig. 14

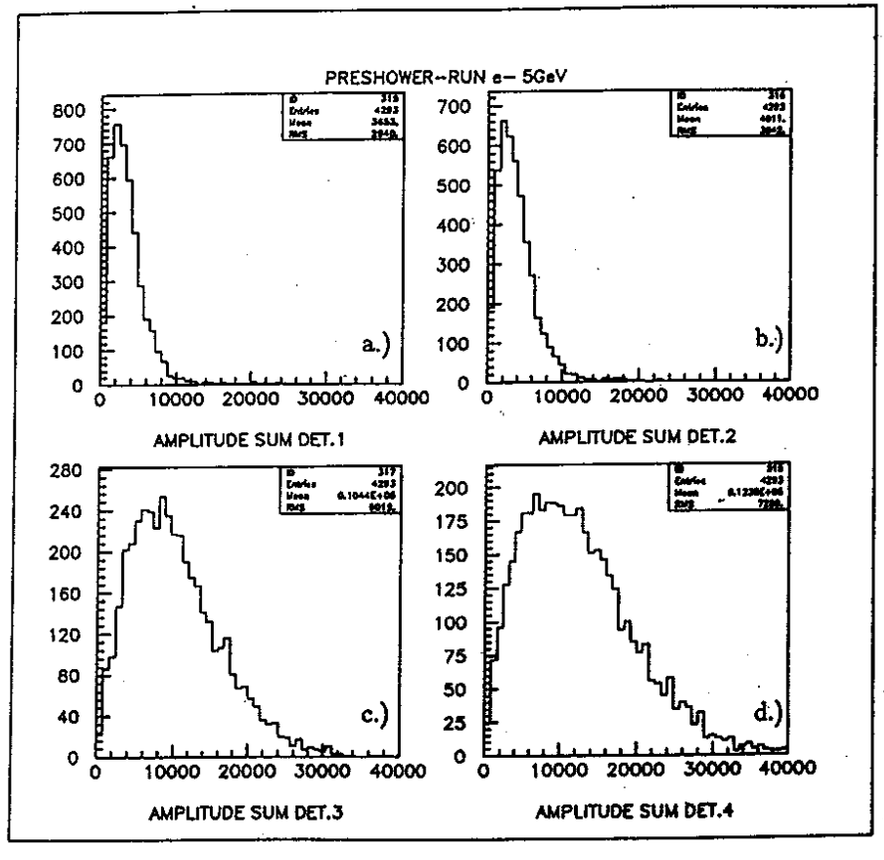
PRESHOWER--RUN e– 5GeV
a.)
b.)
AMPLITUDE SUM DET.1
AMPLITUDE SUM DET.2
c.)
d.)
AMPLITUDE SUM DET.3
AMPLITUDE SUM DET.4

Fig. 15

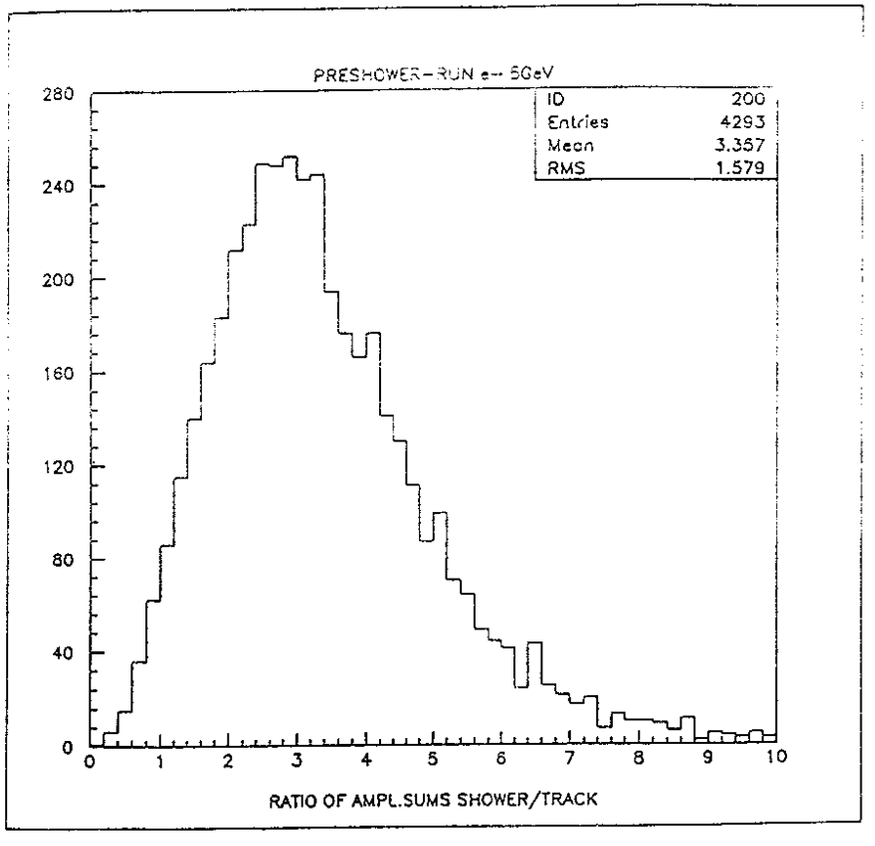
PRESHOWER-RUN e- 5GeV
ID 200
Entries 4293
Mean 3.357
RMS 1.579
280
240
200
160
120
80
40
0
0 1 2 3 4 5 6 7 8 9 10
RATIO OF AMPL.SUMS SHOWER/TRACK

Fig. 16